

Emergence of tension-compression asymmetry from a complete phase-field approach to brittle fracture

Chang Liu, Aditya Kumar*

School of Civil and Environmental Engineering, Georgia Institute of Technology, Atlanta, GA 30332, USA

Abstract

The classical variational approach to brittle fracture propagation does not distinguish between strain energy accumulation in tension versus compression and consequently results in physically unrealistic cracking under compression. A variety of energy splits have been proposed as a possible remedy. However, a unique energy split that can describe this asymmetry for general loading conditions has not been found. The main objective of this paper is to show that a complete phase-field theory of brittle fracture nucleation and propagation, one that accounts for the material strength at large, can naturally capture the tension-compression asymmetry without an energy split. One such theory has been recently proposed by Kumar et al. (2018). Over the past few years, several studies have shown that this theory is capable of accurately describing fracture nucleation and propagation for materials soft and hard under arbitrary monotonic loading conditions. However, a systematic study of the tension-compression asymmetry that emerges from this theory has not yet been reported. This paper does precisely that. In particular, this paper reports a comprehensive study of crack propagation in two problems, one involving a symmetric tension-compression state and the other involving larger compressive stresses at the crack tip. The results are compared with popular energy splits used in literature. The results show that, remarkably, for the second problem, only the complete theory is able to produce experimentally consistent results.

Key words: Tension-compression asymmetry; Brittle materials; Phase-field regularization; Fracture nucleation; Strength

1. Introduction

The mathematical reformulation of Griffith's [1] original idea for fracture by Francfort and Marigo [2] has led to an elegant theory of fracture propagation called the variational theory of brittle fracture. In this theory, the calculation of the fracture state is viewed as a minimization problem for the sum of the bulk strain energy and surface fracture energies with arbitrary add-cracks as one of the test fields. The variational theory can predict both when a large pre-existing crack starts to propagate and how it propagates. Phase-field models [3], developed as a regularization of the variational theory to make it more amenable to numerical studies, retained the elegance of the sharp theory and have proved to be a successful approach to simulate fracture propagation. However, they also inherited a significant shortcoming of the variational theory – they do not distinguish between strain energy accumulation in tension and compression. Consequently, they can not describe the tension-compression asymmetry in fracture response, resulting in cracks under compression.

The popular remedial approach is to split or decompose the strain energy into a positive (opening) and negative (closing) part where only the positive energy drives the evolution of the scalar phase field variable. The energy split approach keeps the variational nature of the classical phase-field model. However, this

*Corresponding author

Email addresses: clicu723@gatech.edu (Chang Liu), aditya.kumar@ce.gatech.edu (Aditya Kumar)

approach suffers from several shortcomings. First, it is not apparent how a unique split can be constructed for a linear elastic isotropic material [4, 5], much less for an anisotropic material [6, 7] or a finite elastic material [8, 9]. Second, many of the popular methods of energy splits are prone to having non-zero residual stiffness in the cracked regions [10]. But perhaps most importantly, no single energy split has been yet shown in the literature to be able to comprehensively describe the tension-compression asymmetry for all loading conditions, static or dynamic [11, 12, 10].

An alternative and more natural solution may arise from the generalized approach of Kumar et al. [13, 14] to phase-field modeling of nucleation and propagation of brittle fracture. In a nutshell, this theory generalizes the classical phase-field theory for fracture propagation by accounting for nucleation in general through the material’s strength surface, while keeping undisturbed the ability of the classical phase-field regularization to model crack propagation according to Griffith’s fracture postulate. A string of recent works [15, 14, 16, 17, 18, 19] have provided a wide range of validation results for a broad spectrum of materials (silicone, titania, graphite, polyurethane, PMMA, alumina, natural rubber, glass, rock), specimen geometries (with large and small pre-existing cracks, V notches, U notches, and smooth boundaries), and loading conditions suggesting that this theory may indeed provide a complete framework for elastic brittle materials. Because the theory accounts for the strength of the material at large, it has been conjectured that it can account for tension-compression asymmetry naturally [14].

Some evidence in this direction has been presented before in previous works for crack nucleation in the absence of pre-existing cracks. The theory was able to provide qualitative and quantitative agreement with the experiments for the indentation test [18] and Brazilian fracture test [19] – problems that both involve large compressive stresses. However, it remains understudied whether the theory can describe the asymmetry under general loading conditions and whether it depends on any model parameters. It is also understudied whether it performs better than the energy split methods for problems involving large pre-existing cracks. The main purpose of this paper is to address these questions. We do so by studying two prominent examples of fracture propagation in which the correct modeling of asymmetry plays an important role.

In the first example, we focus on the mode II fracture of a plate under a quasi-static simple shear loading. This is a benchmark problem for tension-compression asymmetry studied in many previous works [20, 5]. It involves a symmetric tension-compression state in front of the crack. All energy split methods proposed in the literature can predict the correct crack path for this problem. In the second example, we study the propagation from two inclined cracks in a plate under uniaxial compression. The rationale for our choice to study this problem is threefold. First, this problem is of broad interest in rock mechanics and has been extensively studied. Second, it involves an asymmetric tension-compression state at the crack tip with significantly larger compressive stresses. Third, the analysis of this problem with the phase-field method utilizing the conventional energy splits has proved to be technically challenging [21]. It has been claimed in the literature that the experimental crack path can only be obtained by assuming a mode-dependent fracture toughness for the material [21, 22, 23] and more involved splits have been proposed as a solution. We begin in Section 2 by summarizing the general fracture theory of Kumar et al. (2018, 2022). We then present in Sections 3 and 4 a comprehensive study of the two examples. Lastly, some final comments are recorded in Section 5.

2. The complete phase-field theory of brittle fracture of Kumar et al. (2018, 2020)

Consider a structure made of an isotropic linear elastic brittle material occupying an open bounded domain $\Omega \subset \mathbb{R}^3$, with boundary $\partial\Omega$ in its undeformed and stress-free configuration at time $t = 0$. At a later time $t \in (0, T]$, due to an externally applied displacement $\bar{\mathbf{u}}(\mathbf{X}, t)$ on a part $\partial\Omega_{\mathcal{D}}$ of the boundary and a traction $\bar{\mathbf{t}}(\mathbf{X}, t)$ on the complementary part $\partial\Omega_{\mathcal{N}} = \partial\Omega \setminus \partial\Omega_{\mathcal{D}}$, the structure experiences a deformation field $\mathbf{u}(\mathbf{X}, t)$. We write the infinitesimal strain tensor as

$$\mathbf{E}(\mathbf{u}) = \frac{1}{2}(\nabla\mathbf{u} + \nabla\mathbf{u}^T).$$

Non-interpenetration constraint implies that $\det(\mathbf{I} + \nabla\mathbf{u}) > 0$. In response to the externally applied mechanical stimuli, cracks can also nucleate and propagate in the structure. Those are described in a regularized

way by the phase field

$$v = v(\mathbf{X}, t)$$

taking values in $[0, 1]$. Precisely, $v = 1$ identifies regions of the sound material, whereas $v < 1$ identifies regions of the material that have been fractured.

2.1. Constitutive behavior of the material

For isotropic brittle materials, the mechanical behavior is assumed to be completely characterized by three intrinsic properties of the material: (i) elasticity, (ii) strength, and (iii) critical energy release rate.

Elasticity. The elastic behavior for an isotropic linear elastic material is characterized by the stored-energy function

$$W(\mathbf{E}(\mathbf{u})) = \mu \mathbf{E} \cdot \mathbf{E} + \frac{\lambda}{2} (\text{tr } \mathbf{E})^2, \quad (1)$$

where $\mu > 0$ and $\lambda > -2/3\mu$ are the Lamé constants. Recall the basic relations $\mu = E/(2(1 + \nu))$ and $\lambda = E\nu/((1 + \nu)(1 - 2\nu))$, where E is the Young's modulus and ν is the Poisson's ratio. The stress-strain relation is given by

$$\boldsymbol{\sigma}(\mathbf{X}, t) = \frac{E}{1 + \nu} \mathbf{E} + \frac{E\nu}{(1 + \nu)(1 - 2\nu)} (\text{tr } \mathbf{E}) \mathbf{I}$$

Strength. When a macroscopic piece of an elastic brittle material is subjected to an arbitrary but uniform state of stress $\boldsymbol{\sigma}$, fracture nucleates at a critical value of the applied stress. The set of all such stresses defines a surface in the stress space – called a strength surface

$$\mathcal{F}(\boldsymbol{\sigma}) = 0, \quad (2)$$

where $\boldsymbol{\sigma}$ stands for the Cauchy stress tensor. A popular, but not general, choice for the strength surface of the material is the Drucker-Prager strength surface

$$\mathcal{F}(\boldsymbol{\sigma}) = \sqrt{J_2} + \gamma_1 I_1 + \gamma_0 = 0 \quad \text{with} \quad \begin{cases} \gamma_0 = -\frac{2\sigma_{\text{cs}}\sigma_{\text{ts}}}{\sqrt{3}(\sigma_{\text{cs}} + \sigma_{\text{ts}})} \\ \gamma_1 = \frac{\sigma_{\text{cs}} - \sigma_{\text{ts}}}{\sqrt{3}(\sigma_{\text{cs}} + \sigma_{\text{ts}})} \end{cases}, \quad (3)$$

where

$$I_1 = \text{tr } \boldsymbol{\sigma} \quad \text{and} \quad J_2 = \frac{1}{2} \text{tr } \boldsymbol{\sigma}_D^2 \quad \text{with} \quad \boldsymbol{\sigma}_D = \boldsymbol{\sigma} - \frac{1}{3} (\text{tr } \boldsymbol{\sigma}) \mathbf{I} \quad (4)$$

stand for two of the standard invariants of the stress tensor $\boldsymbol{\sigma}$, while the constants $\sigma_{\text{ts}} > 0$ and $\sigma_{\text{cs}} > 0$ denote the uniaxial tensile and compressive strengths of the material. This two-material-parameter Drucker-Prager strength surface (1952) is arguably the simplest model that has proven capable of describing reasonably well the strength of many nominally brittle materials and has been used extensively in previous phase-field studies [14, 16, 18, 19]. We emphasize that the strength surface only defines the crack nucleation under uniform stress states. More precisely, it defines when the phase field v ceases to be 1 under uniform stress states. Under non-uniform stress states, the violation of the strength surface is not a sufficient condition for crack nucleation and requires the contribution of the third intrinsic property: critical energy release rate.

Critical energy release rate. The critical energy release rate (or intrinsic fracture toughness), G_c describes the total energy expended in creating unit fracture surface area. It captures the resistance to the growth of a pre-existing crack. For an isotropic brittle material, G_c is a scalar material constant.

2.2. The governing equations of deformation and fracture

According to the theory of Kumar et al. (2018), the displacement field $\mathbf{u}_k(\mathbf{X}) = \mathbf{u}(\mathbf{X}, t_k)$ and phase field $v_k(\mathbf{X}) = v(\mathbf{X}, t_k)$ at any material point $\mathbf{X} \in \bar{\Omega}$ and discrete time $t_k \in \{0 = t_0, t_1, \dots, t_m, t_{m+1}, \dots, t_M = T\}$ are determined by the system of coupled partial differential equations (PDEs)

$$\begin{cases} \text{Div} \left[v_k^2 \frac{\partial W}{\partial \mathbf{E}}(\mathbf{E}(\mathbf{u}_k)) \right] = \mathbf{0}, & \mathbf{X} \in \Omega, \\ \mathbf{u}_k = \bar{\mathbf{u}}(\mathbf{X}, t_k), & \mathbf{X} \in \partial\Omega_{\mathcal{D}}, \\ \left[v_k^2 \frac{\partial W}{\partial \mathbf{E}}(\mathbf{E}(\mathbf{u}_k)) \right] \mathbf{N} = \bar{\mathbf{t}}(\mathbf{X}, t_k), & \mathbf{X} \in \partial\Omega_{\mathcal{N}} \end{cases} \quad (5)$$

and

$$\begin{cases} \varepsilon G_c \Delta v_k = \frac{8}{3} v_k W(\mathbf{E}(\mathbf{u}_k)) - \frac{4}{3} c_e(\mathbf{X}, t_k) - \frac{G_c}{2\varepsilon}, & \text{if } v_k(\mathbf{X}) < v_{k-1}(\mathbf{X}), \quad \mathbf{X} \in \Omega \\ \varepsilon G_c \Delta v_k \geq \frac{8}{3} v_k W(\mathbf{E}(\mathbf{u}_k)) - \frac{4}{3} c_e(\mathbf{X}, t_k) - \frac{G_c}{2\varepsilon}, & \text{if } v_k(\mathbf{X}) = 1 \text{ or } v_k(\mathbf{X}) = v_{k-1}(\mathbf{X}) > 0, \quad \mathbf{X} \in \Omega \\ v_k(\mathbf{X}) = 0, & \text{if } v_{k-1}(\mathbf{X}) = 0, \quad \mathbf{X} \in \Omega \\ \nabla v_k \cdot \mathbf{N} = 0, & \mathbf{X} \in \partial\Omega \end{cases} \quad (6)$$

with $\mathbf{u}(\mathbf{X}, 0) \equiv \mathbf{0}$ and $v(\mathbf{X}, 0) \equiv 1$, where $\nabla \mathbf{u}_k(\mathbf{X}) = \nabla \mathbf{u}(\mathbf{X}, t_k)$, $\nabla v_k(\mathbf{X}) = \nabla v(\mathbf{X}, t_k)$, $\Delta v_k(\mathbf{X}) = \Delta v(\mathbf{X}, t_k)$, and where $\varepsilon > 0$ is a regularization or localization length and $c_e(\mathbf{X}, t)$ is a driving force containing information about material's strength. The specific constitutive prescription for c_e depends on the particular form of the strength surface and is spelled out below for the case of Drucker-Prager strength surfaces.

Remark 1. The inequalities in (6) describe the constraint that phase field is constrained between 0 and 1 and the classical assumption that fracture is an irreversible process. Moreover, the localization length ε in (6) is purely a regularization parameter that is set to be smaller than the smallest characteristic length scale in the structural problem at hand. In practice, it is also set to be no larger than the material's characteristic fracture length scale.

Remark 2. The computational implementation of the equations (5)–(6) differs from the implementation of the classical variational model only through the presence of the term c_e on the right-hand side of the PDE for the phase-field (6). Accordingly, the standard finite-element staggered scheme can be utilized to solve these equations. In absence of the c_e term in (6), the equations (5)–(6) represent the classical AT₁ phase-field model [24, 25].

Remark 3. The solution of the equations (5)–(6) may be suspect to material interpenetration under compression, unless geometrical nonlinearity through finite kinematics is utilized [13]. In this work, we assume geometrical linearity and only check *a posteriori* that the non-interpenetration constraint is satisfied.

2.3. The model for the external driving force c_e

The external driving force is a manifestation of the presence of the inherent defects in the material, that is, its strength surface at large. Hence, the information about the strength surface enters the governing PDEs through c_e . A blueprint for constructing c_e was outlined in [14]. The construction process specifies that c_e takes the same functional form as the strength surface, in this case, the Drucker-Prager strength surface (3), but with ε -dependent coefficients. Precisely, it is defined as

$$c_e(\mathbf{X}, t) = \hat{c}_e(I_1, J_2; \varepsilon) = \beta_2^\varepsilon \sqrt{J_2} + \beta_1^\varepsilon I_1 + \beta_0^\varepsilon, \quad (7)$$

where

$$\begin{cases} \beta_0^\varepsilon = \delta^\varepsilon \frac{3G_c}{8\varepsilon} \\ \beta_1^\varepsilon = - \left(\frac{(1 + \delta^\varepsilon)(\sigma_{cs} - \sigma_{ts})}{2\sigma_{cs}\sigma_{ts}} \right) \frac{3G_c}{8\varepsilon} + \frac{\sigma_{cs} - \sigma_{ts}}{2E} \\ \beta_2^\varepsilon = - \left(\frac{\sqrt{3}(1 + \delta^\varepsilon)(\sigma_{cs} + \sigma_{ts})}{2\sigma_{cs}\sigma_{ts}} \right) \frac{3G_c}{8\varepsilon} + \frac{\sqrt{3}(\sigma_{cs} + \sigma_{ts})}{2E} \end{cases}, \quad (8)$$

I_1 and J_2 stand for the invariants (4) of the Cauchy stress

$$\boldsymbol{\sigma}(\mathbf{X}, t) = v^2 \frac{\partial W}{\partial \mathbf{E}}(\mathbf{E}(\mathbf{u}))$$

and, hence, read as

$$I_1 = (3\lambda + 2\mu)v^2 \text{tr } \mathbf{E}(\mathbf{u}) \quad \text{and} \quad J_2 = 2\mu^2 v^4 \text{tr } \mathbf{E}_D^2(\mathbf{u})$$

with $\mathbf{E}_D(\mathbf{u}) = \mathbf{E}(\mathbf{u}) - 1/3 (\text{tr } \mathbf{E}(\mathbf{u})) \mathbf{I}$ in terms of the displacement field \mathbf{u} and phase field v , and where δ^ε is a unitless ε -dependent coefficient. The value of δ^ε needs to be calibrated to retain Griffith-fracture propagation with the equations (5)–(6). Currently, the simplest procedure to calibrate δ^ε is to solve, for a given set of material constants E , ν , G_c , σ_{ts} , σ_{cs} , and a given finite localization length ε , a single boundary-value problem of choice for which the nucleation from a large pre-existing crack can be determined analytically and then adjust δ^ε so that the phase-field theory matches the analytical solution. An analytical formula for δ^ε is under development.

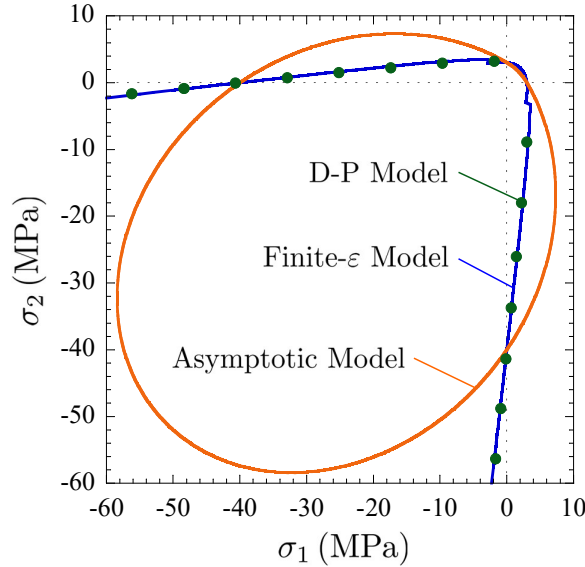


Figure 1: The strength surfaces in the (σ_1, σ_2) -space for stress states with $\sigma_3 = 0$ for gypsum (see Section 4) and localization length $\varepsilon = 1$ mm, as predicted by the driving force introduced in Kumar et al. (2020), named Asymptotic Model, and the driving force introduced in Kumar et al. (2022), named Finite- ε Model. For direct comparison, the Drucker–Prager strength surface (6) is also included.

A correction to the form for c_e was presented in Kumar et al. [18] to improve the description of the compressive part of the strength surface from the governing PDEs (5)–(6) for large values of localization lengths ε . Specifically, this form of c_e is defined as

$$c_e(\mathbf{X}, t) = \hat{c}_e(I_1, J_2; \varepsilon) = \beta_2^\varepsilon \sqrt{J_2} + \beta_1^\varepsilon I_1 + \beta_0^\varepsilon + \frac{1}{v^3} \left(1 - \frac{\sqrt{I_1^2}}{I_1} \right) \left(\frac{J_2(1 + \nu)}{E} + \frac{I_1^2(1 - 2\nu)}{6E} \right), \quad (9)$$

where

$$\begin{cases} \beta_0^\varepsilon = \delta^\varepsilon \frac{3G_c}{8\varepsilon} \\ \beta_1^\varepsilon = - \left(\frac{(1 + \delta^\varepsilon)(\sigma_{cs} - \sigma_{ts})}{2\sigma_{cs}\sigma_{ts}} \right) \frac{3G_c}{8\varepsilon} + \frac{\sigma_{ts}}{2E} \\ \beta_2^\varepsilon = - \left(\frac{\sqrt{3}(1 + \delta^\varepsilon)(\sigma_{cs} + \sigma_{ts})}{2\sigma_{cs}\sigma_{ts}} \right) \frac{3G_c}{8\varepsilon} + \frac{\sqrt{3}\sigma_{ts}}{2E} \end{cases}, \quad (10)$$

The last term is the correction term that is zero when $I_1 > 0$ and non-zero when $I_1 < 0$. In the limit of $\varepsilon \searrow 0$, the correction term is negligible as it is $O(\varepsilon^0)$ and the original model (7) is asymptotically obtained. We refer to the form (7) for c_a as the ‘Asymptotic Model’ and the form (9) as the ‘Finite- ε Model’ in the text below. A direct comparison between the strength surface implied from the two models is shown in Figure 1. The results are shown for gypsum studied in Section 4 with $\varepsilon = 1$ mm. The figure also includes the Drucker-Prager strength surface 3 for comparison. It can be clearly observed that the Finite- ε Model provides a better approximation of Drucker-Prager strength surface than the Asymptotic Model for this value of ε .

3. The simple shear problem

In this section, we deploy the phase-field theory (5)–(6) to do a numerical study of a rectangular specimen with a pre-existing crack, subjected to simple shear loading. This is considered a benchmark problem to investigate tension-compression asymmetry of phase-field models [20, 5]. Fig 2 shows a schematic of the initial geometry of the specimen and applied boundary conditions, as well as the expected crack path normal to the direction of tensile principal stress. The classical phase-field model without an energy split [3, 20] predicts an invalid branching of the pre-existing crack into a tension crack and a compression crack. However, models with energy splits are all able to capture the correct crack path.

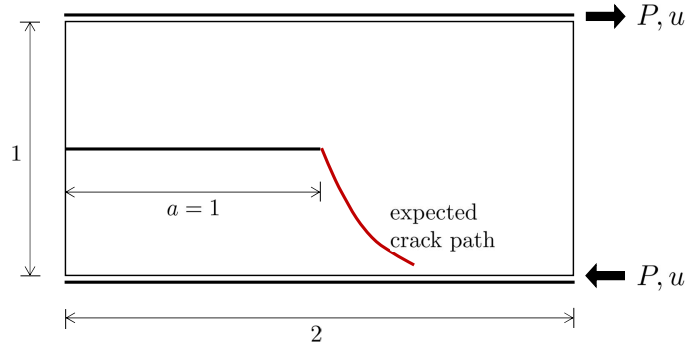


Figure 2: Schematics of the initial specimen geometry and boundary conditions for a pre-notched sample under simple shear. The expected crack path is shown in red.

Following [5], we set Young’s modulus E and Poisson’s ratio ν to be 210 GPa and 0.3 respectively, while the critical energy release rate G_c is set to 2700 N/m. The tensile strength σ_{ts} is fixed to be 3.26 GPa and the compressive strength σ_{cs} is varied. With these material parameters, the value of the classical material’s characteristic length for the AT₁ model is $(3EG_c)/(8\sigma_{ts}^2) = 0.02$ mm [25]. Table 1 provides the values of the regularization length ε , the finite element mesh size h , and the corresponding values of the parameter δ^ε for all the results presented below with the Asymptotic Model (7) and Finite- ε Model (9) for the driving force c_a .

Brittle materials typically have a ratio of compressive strength to tensile strength greater than 3. Hence, with the Asymptotic Model, we first investigate the case when $\sigma_{cs}/\sigma_{ts} = 3$. Figure 3 presents snapshots of the phase field v predicted by the theory at different values of applied displacement for two values of

Table 1: Values of the regularization length ε , FE mesh size h , and the parameter δ^ε utilized in the simulations of simple shear problem.

Model for c_e	σ_{cs}/σ_{ts}	ε (mm)	Mesh size h (mm)	δ^ε
Asymptotic Model (7)	3	0.015	0.0020	1.1
	3	0.01	0.0013	2.15
	1.5	0.015	0.0020	0.4
	1.5	0.01	0.0013	1.15
	1.5	0.0075	0.00075	2.6
Finite- ε Model (9)	1.5	0.015	0.002	-0.03
	1.5	0.0075	0.00075	2.1

localization lengths $\varepsilon = 0.015$ mm and $\varepsilon = 0.01$ mm. We observe that the theory predicts the physically expected crack path for both values of ε and the results are independent of ε . The compression crack is suppressed naturally in this case due to the tension-compression asymmetry built into the theory by accounting for the entire strength surface of the material. Similar results are obtained for all cases with $\sigma_{cs}/\sigma_{ts} > 3$.

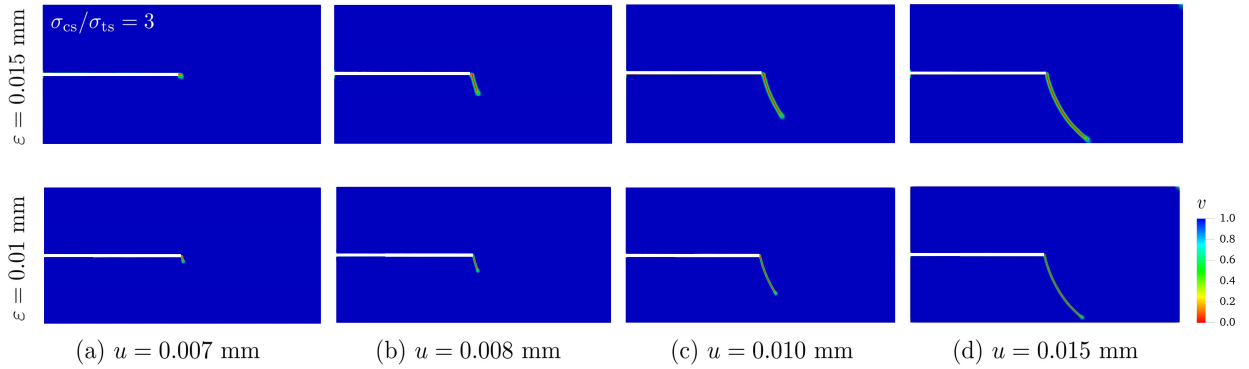


Figure 3: Contour plots of the phase field v predicted by the theory with the Asymptotic Model for driving force c_e for $\sigma_{cs}/\sigma_{ts} = 3$ and two values of localization length, $\varepsilon = 0.015, 0.01$ mm. Results are shown for four values of applied displacement: (a) $u = 0.007$ mm, (b) $u = 0.008$ mm, (c) $u = 0.010$ mm, and (d) $u = 0.015$ mm.

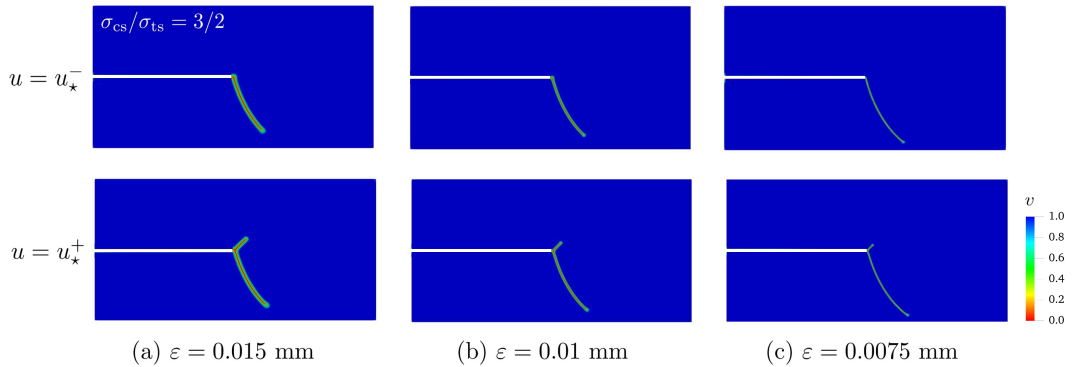


Figure 4: Contour plots of the phase field v predicted by the Asymptotic Model for driving force c_e for $\sigma_{cs}/\sigma_{ts} = 3/2$ at displacements just smaller and just larger than the critical displacement, u_* at which the compression crack nucleates. Results are shown for three localization lengths: (a) $\varepsilon = 0.015$ mm, (b) $\varepsilon = 0.01$ mm, and (c) $\varepsilon = 0.0075$ mm.

Next, we study a case where compressive strength is of similar value as tensile strength to investigate

the limits of the Asymptotic Model. We set $\sigma_{cs}/\sigma_{ts} = 1.5$ and carry out simulations for three values of localization length $\varepsilon = 0.015, 0.01$ and 0.0075 mm. We observe that while initially, only a tension crack nucleates and propagates like the previous case, a compression crack eventually nucleates from the pre-existing crack. Figure 4 shows the contour plots of phase field v for all three values of ε at two instants: shortly before and shortly after the compression crack nucleates. The compression crack nucleates for all three cases, however, it is observed visually that the tension crack propagates more before the compression crack nucleates as the value of ε is decreased. Further evidence for this observation is provided by a plot of reaction force P as a function of applied displacement in Figure 5(a). It is plain from this plot that lowering the value of ε has a substantial impact on the critical applied displacement at which compression crack nucleates. The plot of the implied strength surface for the three values of ε also shows non-convergence. A prohibitively small value of localization length is likely required to get a converged and physically realistic solution.

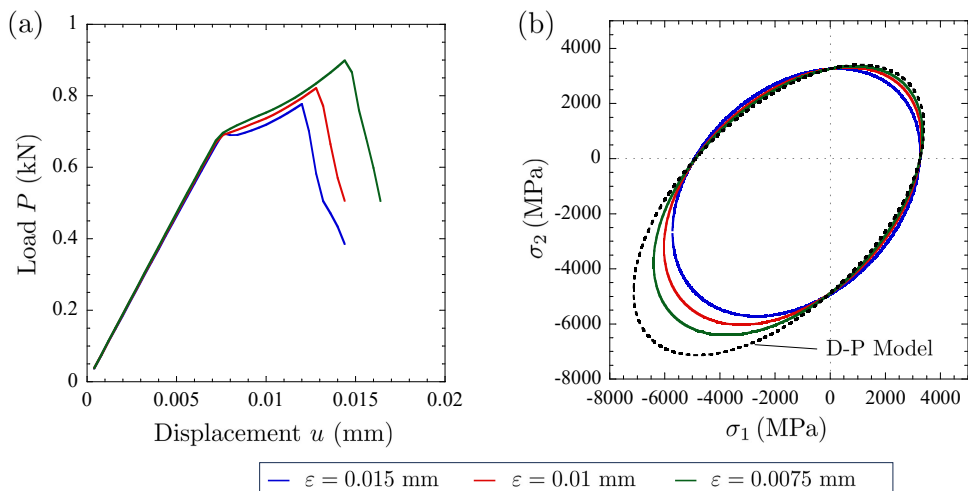


Figure 5: (a) Load-displacement curves and (b) strength surface with the Asymptotic Model for driving force for three values of localization lengths $\varepsilon = 0.015, 0.01$ and 0.0075 mm.

Our previous results for indentation and Brazilian fracture problems have shown that the Finite- ε Model for driving force does not suffer from the same limitations. To verify, we carry out the simulations with that model for $\sigma_{cs}/\sigma_{ts} = 1.5$ and the lowest value of localization length, $\varepsilon = 0.0075$ mm, adopted in the simulations with the Asymptotic Model. The contour plots for the phase-field v are plotted in Figure 6 (a). No compression crack is observed to nucleate. A simulation is also carried out for a higher value of localization length, $\varepsilon = 0.015$ mm, as shown in Figure 6 (b). The absence of a compression crack in that result indicates that the Finite- ε Model can even be used with larger values of ε . The results with larger values of σ_{cs}/σ_{ts} with the Finite- ε Model are not included here, but the same conclusions can be drawn from them.

It is plain from these simulations that while the Asymptotic Model can capture tension-compression asymmetry naturally in problems involving symmetric tension and compression states for realistic values of σ_{cs}/σ_{ts} for brittle materials, it fails to achieve that for comparable values of σ_{cs} and σ_{ts} with finite values of ε . The Finite- ε Model in contrast is more robust and can describe the asymmetry for any values of σ_{cs}/σ_{ts} and ε . Recall that this model is identical to the Asymptotic Model in the limit $\varepsilon \searrow 0$.

4. The wing cracks problem

Next, we confront the theory (5)–(6) and the two models for driving force c_e (7, 9) with a problem of crack nucleation from pre-existing cracks involving large global compressive forces. Fig 7(a) shows a schematic of the initial geometry of the specimen and applied boundary conditions. In this popular test

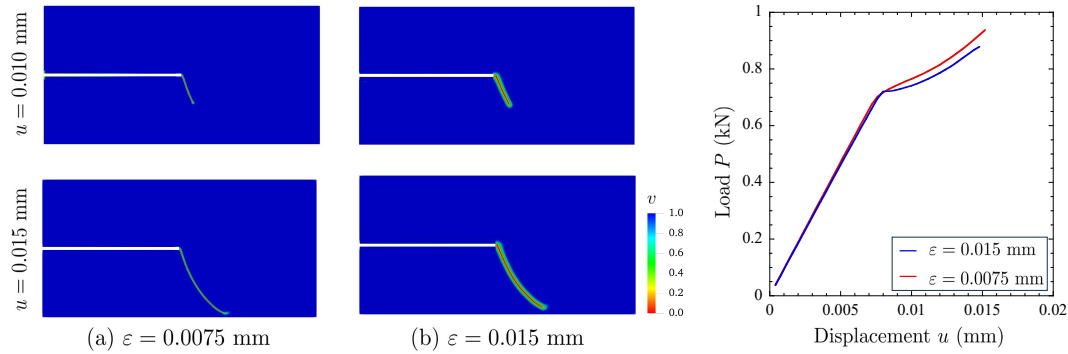


Figure 6: Contour plots of the phase field v predicted by the theory with the Finite- ε Model for driving force c_ε for $\sigma_{cs}/\sigma_{ts} = 3/2$ and two values of localization length: (a) $\varepsilon = 0.0075$ mm and (b) $\varepsilon = 0.015$ mm. Load-displacement curves for both values of ε are shown on the right.

for rock-type materials, a rectangular specimen with two (one or more) inclined cracks is subjected to uniaxial compression. Experimental observations [26, 27, 28, 29] show that the so-called wing cracks (inner and outer) nucleate from existing cracks under this loading; see Fig 7(b). The wing crack nucleation has been extensively studied in the literature and several authors have theoretically and experimentally shown that when and how wing cracks nucleate is significantly affected by the friction between the crack faces [30, 31, 32, 26]. In this work, for computational ease, we assume no friction and no normal contact between the crack faces, consistent with an open flaw assumption. The experimental observations have also indicated that secondary shear cracks may nucleate later resulting in coalescence of the two initial cracks.

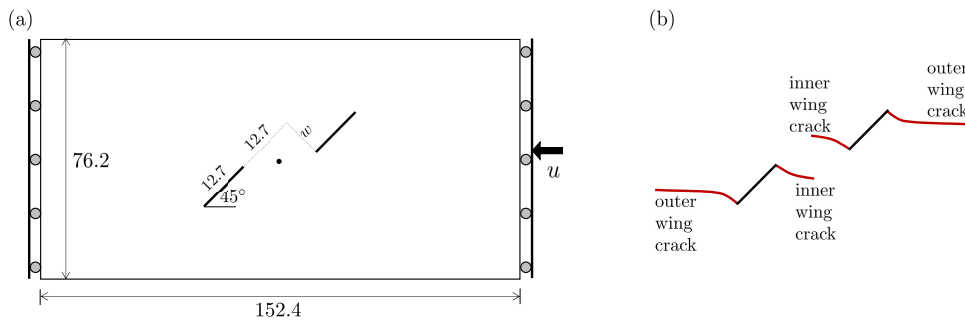


Figure 7: Schematics of the initial specimen geometry and boundary conditions for the wing cracks evolution problem. The expected inner and outer wing crack paths based on experimental observations are shown on the right.

Several authors have also investigated this problem with the classical phase-field method [21, 22, 33, 34, 23] and have noted the inability of the classical energy split techniques, in particular, the two most popular energy split techniques – volumetric-deviatoric and spectral, to accurately describe the crack paths observed in the experiments. For direct comparison, we first simulated this problem with the classical model and the typical energy splits. We adopt representative values of material parameters for gypsum [23]. Young’s modulus E , Poisson’s ratio ν , and critical energy release rate G_c are set to 5.96 GPa, 0.15 and 10 N/m respectively. The localization length ε is chosen to be 1 mm. The separation between the cracks, w , is taken as 6.35 mm.

The results are demonstrated in Figure 8(a)-(c). It is plain from these results these classical energy splits perform poorly for this problem. Volumetric-deviatoric split leads to compression cracks. The recently introduced star-convex model [10] as a variation on the volumetric-deviatoric split would show similar compression cracks. The results with spectral split show outer wing cracks, but they appear as artificially wider and distorted presumably due to non-zero residual stresses in the cracked region. Inner wing cracks are not observed at all. These deficiencies of the classical splits under large compressive forces have been

noticed before for the problem of indentation of glass plates with flat-ended indenters [11, 18]. Alternative energy splits have been proposed to resolve these deficiencies. One such split is the modal split of [22], in which the energy is first split based on the different kinematic modes – opening mode and shearing mode. The opening mode energy is taken to be non-zero only when a scalar mode I strain is greater than 0. This energy split, however, predicts a primary shear crack instead of wing cracks when the fracture toughness is mode-independent, see Fig. 8(d) where a result reproduced from [22] is shown. The authors claimed that primary wing cracks can only be obtained when the mode II fracture toughness is much higher than the mode I fracture toughness.

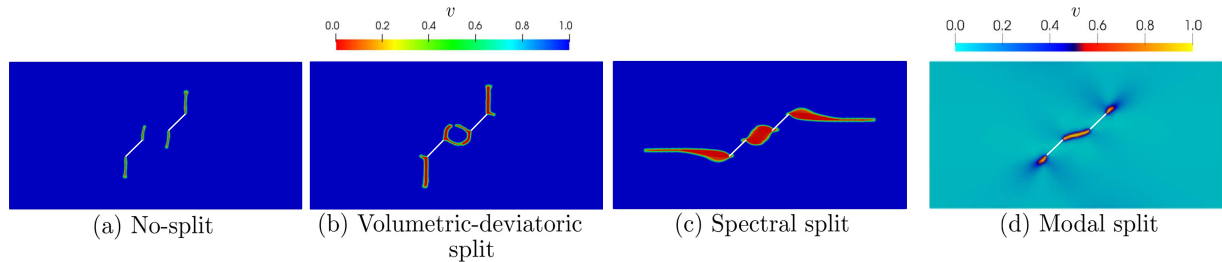


Figure 8: Contour plots of the phase-field v predicted by the (a) classical phase-field (no-split) model, (b) classical phase-field model with volumetric-deviatoric energy split, (c) classical phase-field model with spectral split, and (d) phase-field model with modal split reproduced from Bryant and Sun [22].

To simulate this problem with the theory of Kumar et al. (5)–(6) and the two models for driving force c_e , we fix tensile strength σ_{ts} of gypsum to 3 MPa and we choose the compressive strength as 20 MPa or 40 MPa. The fracture toughness is considered mode-independent. Table 2 provides the values of the regularization length ε , the finite element mesh size h , and the corresponding values of the parameter δ^ε for the results with the theory of Kumar et al. To avoid the possibility of crack face interpenetration, we model the pre-existing cracks as phase-field cracks by setting phase-field v equal to 0 on the crack surfaces. Even so, modeling the cracks as open flaws with a small distance between the crack surfaces yields similar results.

Table 2: Values of the regularization length ε , FE mesh size h , and the parameter δ^ε utilized in the simulations of wing crack problem.

Model for c_e	σ_{cs}/σ_{ts}	ε (mm)	Mesh size h (mm)	δ^ε
Asymptotic Model (7)	40/3	1	0.1	7.5
Finite- ε Model (9)	20/3	1	0.1	3.4
	40/3	1	0.1	3.75

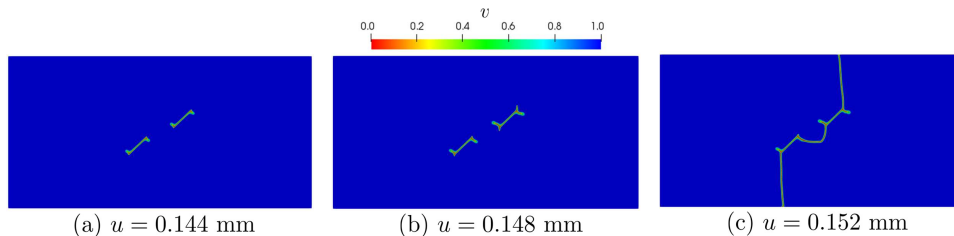


Figure 9: Contour plots of the phase field v predicted by the theory with the Asymptotic Model for driving force c_e for wing crack problem with $w = 6.35$ mm, $\sigma_{cs}/\sigma_{ts} = 40/3$ and $\varepsilon = 1$ mm.

Figure 9 presents results with the Asymptotic Model for c_e with $w = 6.35$ mm. Fig. 9(a) shows that both inner and outer wing cracks initially nucleate in the specimen. However, soon after, compressive cracks nucleate and propagate fast toward the lateral boundary as seen in Fig. 9(b)-(c). Unlike the simple shear

example in Section 3, a larger value of compressive strength does not suppress the nucleation of compressive cracks, however it does delay it.

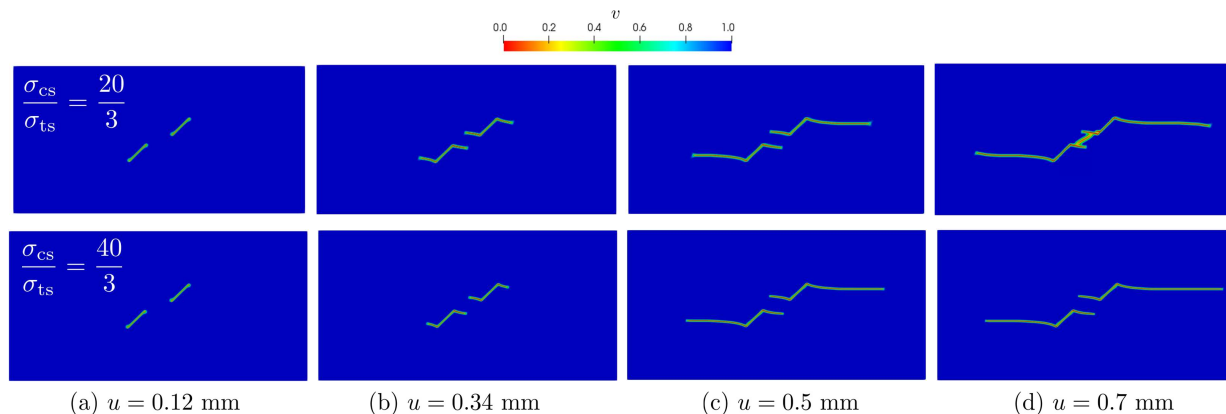


Figure 10: Contour plots of the phase field v predicted by the theory with the Finite- ε Model for driving force c_e for wing crack problem $w = 6.35$ mm, $\varepsilon = 1$ mm and two values for compressive strength to tensile strength ratio: (a) $\sigma_{cs}/\sigma_{ts} = 20/3$ and (b) $\sigma_{cs}/\sigma_{ts} = 40/3$, at four applied displacements u .

Figure 10(a) presents results with the Finite- ε Model for c_e with $\sigma_{cs}/\sigma_{ts} = 20/3$. The contour plots of the phase field v are shown at four values of applied displacements u . Two comments are in order for these results. First, the Finite- ε Model for the driving force is able to capture the experimentally observed inner and outer wing crack paths. We observe that the inner and outer wing cracks nucleate at an applied displacement of $u = 0.12$ mm and stably propagate in the direction of applied loading. Second, the model can also capture the formation of secondary shear cracks and the coalescence of initial cracks. At around $u = 0.7$ mm, a secondary shear crack forms in between the inner wing cracks. However, the coalescence is a brutal crack event, and we experience numerical convergence issues beyond this displacement.

Fig. 10(b) shows the results obtained for $\sigma_{cs}/\sigma_{ts} = 40/3$. The results are qualitatively and quantitatively similar to the case with $\sigma_{cs}/\sigma_{ts} = 20/3$, except that because of the higher compressive strength and consequently higher shear strength, the secondary shear crack supposedly nucleates at a larger displacement than 0.7 mm. For completeness, we also carried out simulations for three different separations between the two pre-existing cracks as done in experimental studies. In each case, we observe inner and outer wing cracks nucleating at roughly the same angle as the base case with $w = 6.35$ mm and propagating in the loading direction towards the center of the left and right boundaries.

5. Final Comments

The two examples presented in this paper add to the validation results presented in previous works on the indentation problem [18] and the Brazilian fracture test [19] which demonstrate that the theory of Kumar et al. (2020) for linear elastic brittle fracture can describe the tension-compression asymmetry in fracture nucleation and propagation under a wide variety of loading and geometrical situations. This work in particular has highlighted the differences between the results from the two models for the driving force that describe the material's strength surface. The first model proposed in Kumar et al. (2020) successfully suppresses compression cracks for realistic brittle materials when the problem involves a symmetric tension-compression state, like the simple shear problem in Section 3. However, for localization lengths ε that are not prohibitively small, it fails in problems involving large compressive forces. The second model proposed in Kumar et al. (2022) to improve the representation of strength surface for finite values of localization length under compressive states proves to be more robust and reliably provides physically consistent results for a wide range of values for ε and compressive strength to tensile strength ratio.

The results presented in Section 4 for the wing cracks problem have also made it plain that a complete model of tension-compression asymmetry with the phase-field models is needed to consistently and uniquely

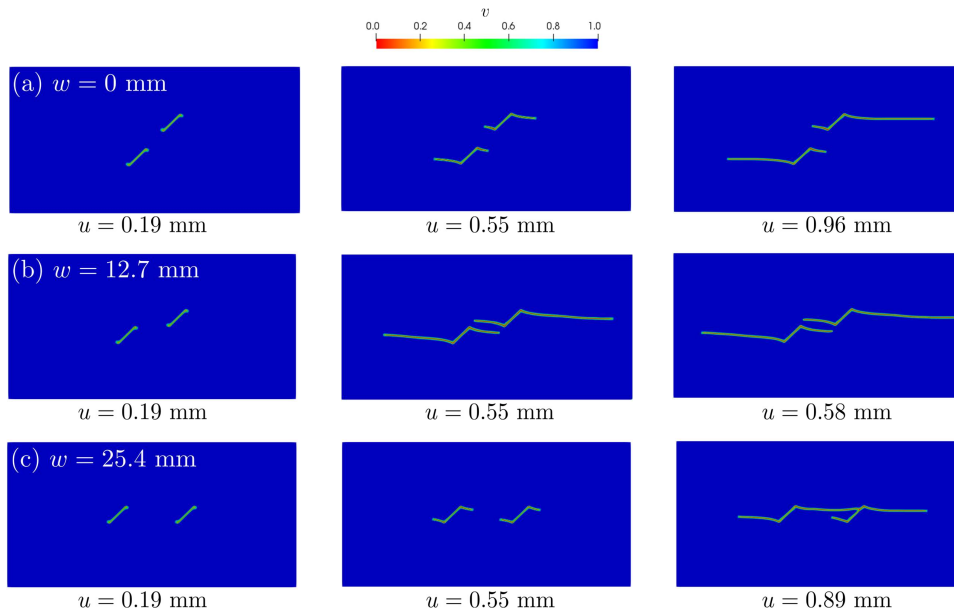


Figure 11: Contour plots of the phase field v for wing crack problem with three different values of separation between the two pre-existing cracks – (a) $w = 0$ mm, (b) $w = 12.7$ mm, and (c) $w = 25.4$ mm – predicted with the Finite- ε Model for driving force c_e .

interpret the fracture toughness from experimental results involving large compression and mixed mode fracture. Future work will investigate further the effect of crack-parallel compressive stresses on fracture nucleation from large pre-existing cracks.

Acknowledgements

The author A. Kumar would like to acknowledge the financial support from the start-up fund provided by the Georgia Institute of Technology.

References

- [1] A. A. Griffith, Vi. the phenomena of rupture and flow in solids, Philosophical transactions of the royal society of london. Series A, containing papers of a mathematical or physical character 221 (1921) 163–198.
- [2] G. A. Francfort, J.-J. Marigo, Revisiting brittle fracture as an energy minimization problem, Journal of the Mechanics and Physics of Solids 46 (1998) 1319–1342.
- [3] B. Bourdin, G. A. Francfort, J.-J. Marigo, Numerical experiments in revisited brittle fracture, Journal of the Mechanics and Physics of Solids 48 (2000) 797–826.
- [4] H. Amor, J.-J. Marigo, C. Maurini, Regularized formulation of the variational brittle fracture with unilateral contact: Numerical experiments, Journal of the Mechanics and Physics of Solids 57 (2009) 1209–1229.
- [5] C. Miehe, F. Welschinger, M. Hofacker, Thermodynamically consistent phase-field models of fracture: Variational principles and multi-field fe implementations, International journal for numerical methods in engineering 83 (2010) 1273–1311.
- [6] N. P. van Dijk, J. J. Espadas-Escalante, P. Isaksson, Strain energy density decompositions in phase-field fracture theories for orthotropy and anisotropy, International Journal of Solids and Structures 196 (2020) 140–153.
- [7] B.-T. Vu, H. Le Quang, Q.-C. He, Modelling and simulation of fracture in anisotropic brittle materials by the phase-field method with novel strain decompositions, Mechanics Research Communications 124 (2022) 103936.
- [8] M. J. Borden, T. J. Hughes, C. M. Landis, A. Anvari, I. J. Lee, A phase-field formulation for fracture in ductile materials: Finite deformation balance law derivation, plastic degradation, and stress triaxiality effects, Computer Methods in Applied Mechanics and Engineering 312 (2016) 130–166.
- [9] S. Tang, G. Zhang, T. F. Guo, X. Guo, W. K. Liu, Phase field modeling of fracture in nonlinearly elastic solids via energy decomposition, Computer Methods in Applied Mechanics and Engineering 347 (2019) 477–494.
- [10] F. Vicentini, C. Zolesi, P. Carrara, C. Maurini, L. de Lorenzis, On the energy decomposition in variational phase-field models for brittle fracture under multi-axial stress states (2023).

- [11] M. Strobl, T. Seelig, Phase field modeling of hertzian indentation fracture, *Journal of the Mechanics and Physics of Solids* 143 (2020) 104026.
- [12] S. Zhang, W. Jiang, M. R. Tonks, Assessment of four strain energy decomposition methods for phase field fracture models using quasi-static and dynamic benchmark cases, *Materials Theory* 6 (2022) 6.
- [13] A. Kumar, G. A. Francfort, O. Lopez-Pamies, Fracture and healing of elastomers: A phase-transition theory and numerical implementation, *Journal of the Mechanics and Physics of Solids* 112 (2018) 523–551.
- [14] A. Kumar, B. Bourdin, G. A. Francfort, O. Lopez-Pamies, Revisiting nucleation in the phase-field approach to brittle fracture, *Journal of the Mechanics and Physics of Solids* 142 (2020) 104027.
- [15] A. Kumar, K. Ravi-Chandar, O. Lopez-Pamies, The configurational-forces view of the nucleation and propagation of fracture and healing in elastomers as a phase transition, *International Journal of Fracture* 213 (2018) 1–16.
- [16] A. Kumar, O. Lopez-Pamies, The phase-field approach to self-healable fracture of elastomers: A model accounting for fracture nucleation at large, with application to a class of conspicuous experiments, *Theoretical and Applied Fracture Mechanics* 107 (2020) 102550.
- [17] A. Kumar, O. Lopez-Pamies, The poker-chip experiments of gent and lindley (1959) explained, *Journal of the Mechanics and Physics of Solids* 150 (2021) 104359.
- [18] A. Kumar, K. Ravi-Chandar, O. Lopez-Pamies, The revisited phase-field approach to brittle fracture: application to indentation and notch problems, *International Journal of Fracture* 237 (2022) 83–100.
- [19] A. Kumar, Y. Liu, J. E. Dolbow, O. Lopez-Pamies, The strength of the brazilian fracture test, *Journal of the Mechanics and Physics of Solids* 182 (2024) 105473.
- [20] B. Bourdin, G. A. Francfort, J.-J. Marigo, The variational approach to fracture, *Journal of elasticity* 91 (2008) 5–148.
- [21] X. Zhang, S. W. Sloan, C. Vignes, D. Sheng, A modification of the phase-field model for mixed mode crack propagation in rock-like materials, *Computer Methods in Applied Mechanics and Engineering* 322 (2017) 123–136.
- [22] E. C. Bryant, W. Sun, A mixed-mode phase field fracture model in anisotropic rocks with consistent kinematics, *Computer Methods in Applied Mechanics and Engineering* 342 (2018) 561–584.
- [23] C. Steinke, J. Storm, M. Kaliske, Energetically motivated crack orientation vector for phase-field fracture with a directional split, *International Journal of Fracture* 237 (2022) 15–46.
- [24] K. Pham, H. Amor, J.-J. Marigo, C. Maurini, Gradient damage models and their use to approximate brittle fracture, *International Journal of Damage Mechanics* 20 (2011) 618–652.
- [25] E. Tanné, T. Li, B. Bourdin, J.-J. Marigo, C. Maurini, Crack nucleation in variational phase-field models of brittle fracture, *Journal of the Mechanics and Physics of Solids* 110 (2018) 80–99.
- [26] A. Bobet, H. Einstein, Fracture coalescence in rock-type materials under uniaxial and biaxial compression, *International Journal of Rock Mechanics and Mining Sciences* 35 (1998) 863–888.
- [27] M. Sagong, A. Bobet, Coalescence of multiple flaws in a rock-model material in uniaxial compression, *International Journal of Rock Mechanics and Mining Sciences* 39 (2002) 229–241.
- [28] H. Lee, S. Jeon, An experimental and numerical study of fracture coalescence in pre-cracked specimens under uniaxial compression, *International Journal of Solids and Structures* 48 (2011) 979–999.
- [29] X.-P. Zhou, J.-Z. Zhang, S.-Q. Yang, F. Berto, Compression-induced crack initiation and growth in flawed rocks: a review, *Fatigue & Fracture of Engineering Materials & Structures* 44 (2021) 1681–1707.
- [30] S. Nemat-Nasser, H. Horii, Compression-induced nonplanar crack extension with application to splitting, exfoliation, and rockburst, *Journal of Geophysical Research: Solid Earth* 87 (1982) 6805–6821.
- [31] H. Horii, S. Nemat-Nasser, Compression-induced microcrack growth in brittle solids: Axial splitting and shear failure, *Journal of Geophysical Research: Solid Earth* 90 (1985) 3105–3125.
- [32] P. S. Steif, Crack extension under compressive loading, *Engineering Fracture Mechanics* 20 (1984) 463–473.
- [33] S. Zhou, X. Zhuang, H. Zhu, T. Rabczuk, Phase field modelling of crack propagation, branching and coalescence in rocks, *Theoretical and Applied Fracture Mechanics* 96 (2018) 174–192.
- [34] T. You, Q.-Z. Zhu, P.-F. Li, J.-F. Shao, Incorporation of tension-compression asymmetry into plastic damage phase-field modeling of quasi brittle geomaterials, *International Journal of Plasticity* 124 (2020) 71–95.